Title
'Beam-emission spectroscopy' diagnostics also measure edge fast-ion light

Journal
Plasma Physics and Controlled Fusion, 53(8)

ISSN
0741-3335

Authors
Heidbrink, WW
McKee, GR
Smith, DR
et al.

Publication Date
2011-08-01

DOI
10.1088/0741-3335/53/8/085007

Plasma Phys. Control. Fusion **53** (2011) 085007 (19pp) doi:10.1088/0741-3335/53/8/085007

'Beam-emission spectroscopy' diagnostics also measure edge fast-ion light

W W Heidbrink[1], G R McKee[2], D R Smith[2] and A Bortolon[1]

[1] Department of Physics and Astronomy, University of California, Irvine, CA, USA
[2] Department of Engineering Physics, University of Wisconsin, Madison, WI, USA

Received 15 December 2010, in final form 8 May 2011
Published 2 June 2011
Online at stacks.iop.org/PPCF/53/085007

Abstract
Beam-emission spectroscopy (BES) diagnostics normally detect fluctuations in the light emitted by an injected neutral beam. Under some circumstances, however, light from fast ions that charge exchange in the high neutral-density region at the edge of the plasma make appreciable contributions to the BES signals. This 'passive' fast-ion D_α (FIDA) light appears in BES signals from both the DIII-D tokamak and the National Spherical Torus Experiment (NSTX). One type of passive FIDA light is associated with classical orbits that traverse the edge. Another type is caused by instabilities that expel fast ions from the core; this light can complicate measurement of the instability eigenfunction.

(Some figures in this article are in colour only in the electronic version)

1. Introduction

Beam-emission spectroscopy (BES) is a diagnostic technique that infers local fluctuations in density $\tilde{n}$ from fluctuations in the light emitted by an injected neutral beam [1]. Although fluctuations in the neutral-beam density induced by fluctuations near the plasma edge can influence the measurement [2], in practice, fluctuations in light intensity are normally proportional to the local density fluctuation at the intersection of the diagnostic sightline with the injected neutral beam. Consequently, BES is a powerful diagnostic of broadband, low wavenumber, turbulence [3]. Another important application is measurement of the eigenfunction of coherent MHD modes [4].

The DIII-D [5] and National Spherical Torus Experiment (NSTX) [6] BES diagnostics measure Doppler-shifted D_α light from injected deuterium neutral beams. Another instrument, the fast-ion D_α (FIDA) diagnostic also measures Doppler-shifted D_α light [7]. FIDA light comes from fast ions that charge exchange with the injected neutral beam, then undergo a Balmer-alpha transition. Because beam emission is generally much brighter than FIDA emission, successful FIDA diagnostics usually select viewing geometries that move the Doppler-shifted beam emission out of the spectral region of interest.

In addition to FIDA, another common fast-ion diagnostic is neutral-particle analysis (NPA). Like FIDA, NPA diagnostics rely on a charge-exchange event between a fast ion and a neutral. When discussing the signal from an NPA, it is customary to distinguish between 'active' charge exchange that occurs with injected neutrals and 'passive' charge exchange that occurs with neutrals in the plasma periphery when the diagnostic beam is off. Typically, the active and passive contributions to the signal are comparable.

All previous publications on FIDA light (reviewed in [8]) utilized the 'active' FIDA light that arises from collisions between fast ions and injected neutrals. (There is also a cloud of thermal 'halo' neutrals that surrounds the beam; for the purposes of the present discussion, reactions with halo neutrals are classified as an active process.) In a typical FIDA installation, any passive FIDA light is included in the background that is subtracted from the total signal to obtain the net (active) signal.

In this paper, we show that passive FIDA light is detected by BES diagnostics under certain circumstances. In the case of virulent fast-ion instabilities, bursts of passive FIDA light can be comparable to the beam emission in intensity. These bursts complicate use of BES to measure the mode structure, although techniques are available to distinguish the FIDA light from the beam emission. The presence of passive FIDA light in BES signals can provide useful information about the fast-ion losses.

The geometry of the BES measurement and estimates of the magnitude of the passive FIDA contribution appear in sections 2 and 3. Beam-ion orbits that traverse the edge in the equilibrium fields can produce passive FIDA light (section 4). Section 5 shows several examples of bursts of passive FIDA light during fast-ion instabilities. The paper concludes with a discussion of the diagnostic implications (section 6).

2. Apparatus

A plan view of the neutral-beam sources and BES sightlines in DIII-D are shown in figure 1(*a*). DIII-D has eight neutral-beam sources that are distributed around the machine; the BES diagnostic views the two 150° sources. (The sources are identified by their toroidal angle.) To provide a well-localized BES density fluctuation measurement, only one of the 150° sources injects at a time. For the data in this paper, 32 channels measure a radial profile along the beam. Each sightline intersects the beam once and crosses the plasma edge twice. The sightlines are arranged so that the beam emission is blue-shifted. Figure 1(*c*) shows a calculation of the beam emission and the spectral window for the bandpass filter that selects the desired blue-shifted radiation. To maximize the signal-to-noise, the filter also collects light from the thermal deuterium charge exchange and halo. The transmission of the filter is $<1\%$ at the unshifted D_α line at 656.1 nm but some cold D_α light does leak through the filter, especially at an ELM. (Oscillations at mode frequencies associated with fast-ion excitation of the cold D_α line [9] are negligible, however.) In the vertical plane, the lens is at $z \simeq 15$ cm above the midplane and views downward at the beam, intersecting the beam near the midplane ($z = 0$).

Similar diagrams for the NSTX installation appear in figures 1(*b*) and (*d*). NSTX has three neutral-beam sources; the BES diagnostic views all three. Each sightline crosses the plasma edge twice. The sightlines are arranged so that the beam emission is red-shifted. To avoid prominent carbon lines at 657.8 and 658.3 nm, the bandpass filter selects a relatively large Doppler shift. Consequently, halo light and cold D_α light make negligible contributions to the NSTX BES signals. In the vertical plane, the lens is 45 cm below the midplane and views upward at the beam in order to match closely the local field line pitch angle.

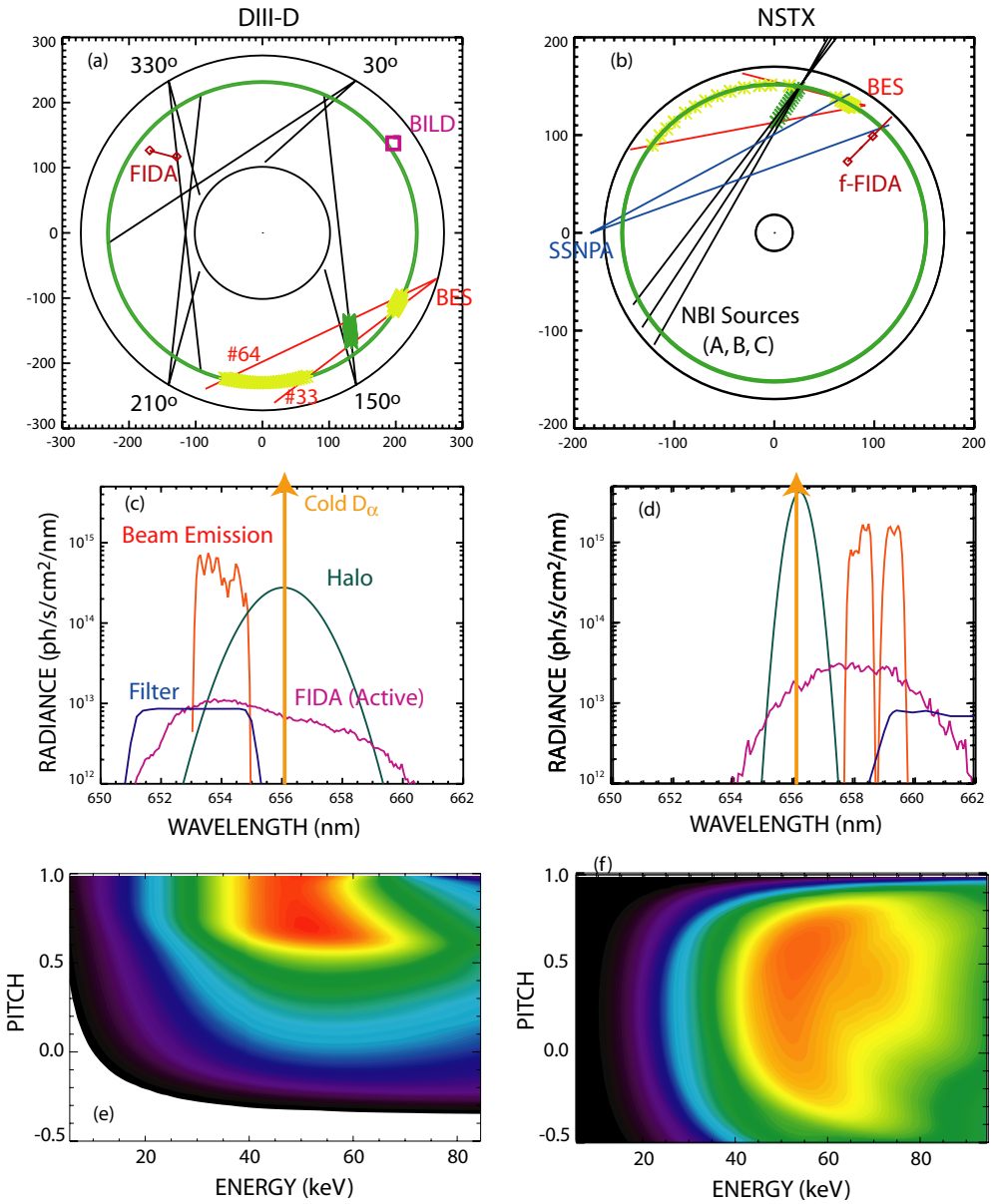

Figure 1. (*a*), (*b*) Plan views of DIII-D (left) and NSTX (right). The beam centerlines for the 8 DIII-D and 3 NSTX neutral-beam sources are shown. For the BES diagnostics, the lines indicate the range of sightlines for the data in this paper; the X symbols represent points of intersection of a sightline with an edge or injected neutral source. Also shown are the toroidal locations of the other fast-ion diagnostics discussed in this paper: the DIII-D BILD detector and FIDA spectrometer, two of the NSTX SSNPA sightlines, and the NSTX reference f-FIDA sightline. (*c*), (*d*) Calculated beam emission, thermal halo, and active FIDA spectra for DIII-D (left) and NSTX (right). The transmission of the BES bandpass filters are also shown. The spectra are computed by the FIDASIM [15] code for the parameters of the DIII-D discharge shown in figure 6 and the NSTX discharge shown in figure 5, respectively. (*e*), (*f*) Sensitivity of different portions of velocity space for the DIII-D BES sightline #33 at the near edge (left) and a central NSTX BES sightline at the near edge (right). A rainbow color scale is employed, with red indicating the largest values.

Each signal from the DIII-D BES diagnostic is separated into a low-pass, approximately dc, 'slow' signal and a high-pass, ac-coupled, 'fast' signal. The associated filter time constant is ∼1 ms. On NSTX, use of higher resolution digitizers accommodates both low- and high-frequency components in a single digitized waveform.

In this paper, the DIII-D beams inject deuterium neutrals at 75–80 keV. The NSTX beams inject deuterium neutrals at 70–90 keV. In both DIII-D and NSTX, the plasma current flows counter-clockwise when viewed from above, while the toroidal field is clockwise. In both devices, co-going fast ions that charge exchange in the BES sightline produce Doppler-shifted radiation with the same sign as the beam emission, so FIDA light from co-going ions is transmitted through the bandpass filter. (For DIII-D, the light is blue-shifted; for NSTX, it is red-shifted.)

To quantify the sensitivity of the BES diagnostic to the fast-ion population, we calculate a fast-ion weight function. (A weight function is a convenient way to characterize the velocity-space dependence of a fast-ion diagnostic [8, 10].) The measured signal is the convolution of the weight function with the fast-ion distribution function. The weight functions for selected BES sightlines are shown for the DIII-D and NSTX cases in figures 1(*e*) and (*f*), respectively. Here, the velocity-space variables that characterize the distribution function are the energy E and pitch $v_\parallel/v$, with positive pitch defined as co-going. Details of the calculation appear in the appendix. The weight functions indicate that co-going fast ions can produce light that is detected by the BES diagnostics. Because of the larger Doppler shift of the bandpass filter, the NSTX weight function is shifted to higher energies than the DIII-D weight function. The large vertical angle for NSTX results in a fairly large angle between the sightline and the field at the plasma edge, so the NSTX views are more sensitive to vertical energies than the DIII-D views.

Figure 1 also shows the locations of several other fast-ion diagnostics. The DIII-D beam-ion loss detectors (BILDs) consist of a pair of foils nestled into a vacuum port just below the midplane ($z \simeq -12$ cm) [11]. One pair of foils measures ions that precess in the co-current direction; the other pair measures counter-current orbits. All data in this paper are from the co-current foil pair at ∼60° (figure 1(*a*)). A vertically viewing FIDA diagnostic at 315° measures the D_α spectrum [12]. Figure 1(*b*) shows the sightlines of two of the chords of the NSTX solid state neutral-particle analyzer (SSNPA) [13] diagnostic. In 2010, this diagnostic was operated in current mode. From the geometry, the diagnostic is sensitive to co-going fast ions that charge exchange in the beam or in the edge region. NSTX is also equipped with a bandpass filter-based 'f-FIDA' diagnostic [14]. The diagnostic has both active sightlines that view a beam and passive sightlines that miss the beam; both sets of views are nearly vertical. The f-FIDA data in this paper are from a reference sightline, so only passive FIDA light contributes to its signal.

3. Intensity estimates

In this section, we estimate the intensities of active FIDA, passive FIDA and beam-emission light and show that it is reasonable to expect detection of passive FIDA light by the BES diagnostics.

The vast majority of FIDA light occurs when a fast ion undergoes a charge-exchange reaction that places it in the $n = 3$ atomic energy level [8]. Thus, the FIDA radiance I_F is

$$I_F \simeq \int \mathrm{d}l \sum n_0 n_f \sigma v f_{3\to 2}. \quad (1)$$

Here, the rate that charge-exchange reactions place fast ions in the $n = 3$ state is represented by $\sum n_0 \sigma v$, where $\sum n_0$ represents a sum over the various neutral populations in their various energy levels and σv is the reactivity (appropriately averaged over the relative velocities). The fraction of excited $n = 3$ neutrals that undergo the measured Balmer-alpha transition is $f_{3\to2} = A_{32}/(A_{32} + A_{31} + \nu_{\rm coll})$, where A_{32} and A_{31} are Einstein coefficients and $\nu_{\rm coll}$ is the rate of collisional losses from the $n = 3$ state. The density of fast ions is $n_{\rm f}$ and the measurement is integrated over the line of sight, $\int {\rm d}l$.

The neutrals that emit beam emission are in collisional–radiative equilibrium and most neutrals are in the ground state, so the beam-emission radiance $I_{\rm B}$ is

$$I_{\rm B} \simeq \int {\rm d}l \sum n_0 \frac{n_3}{n_1} A_{32}, \tag{2}$$

where n_3/n_1 is the fraction of neutrals in the $n = 3$ state. The occupation fraction n_3/n_1 is a function of density, temperature and impurity concentration and is on the order of 10^{-3} for typical parameters.

In the case of active FIDA emission, $\sum n_0$ represents the injected neutrals and their associated halo neutrals. For this case, many terms in equations (1) and (2) are nearly identical. The ratio of active FIDA light $I_{\rm F,A}$ to beam-emission light $I_{\rm B}$ is therefore

$$I_{\rm F,A}/I_{\rm B} \simeq \frac{n_{\rm f}\sigma v}{(n_3/n_1)} \frac{f_{3\to2}}{A_{32}}. \tag{3}$$

At low density, most transitions out of the $n = 3$ state are radiative and the last term in this expression is approximately $1/(A_{32} + A_{31}) \simeq 10^{-8}$ s. In the plasma core, typical values for the fast-ion density $n_{\rm f}$ range from 10^{11} to 10^{12} cm^{-3}. For an 80 keV fast ion, the charge-exchange cross section for a reaction with a ground-state donor neutral that puts the neutralized fast ion in the $n = 3$ state is $\sigma_{1\to3} = 9.4 \times 10^{-18}$ cm^2. In practice, reactions with excited donor neutrals are also important [8], so the effective cross section is a few times larger. Thus, $I_{\rm F,A}/I_{\rm B} \sim 6 \times 10^{-2}$ when $n_{\rm f} = 10^{12}$ cm^{-3}. Figures 1(*c*) and (*d*) show simulations [15] of the expected light intensity from beam emission, halo emission, and active FIDA emission for actual experimental DIII-D and NSTX conditions. As expected, the active FIDA spectral radiance is 1–2 orders of magnitude smaller than the beam emission. Under normal conditions, active FIDA light makes a small contribution to BES signals.

Next, consider the ratio of passive FIDA light $I_{\rm F,P}$ to active FIDA light $I_{\rm F,A}$. Now the terms in equation (1) are different for passive emission than for active emission. The ratio is

$$I_{\rm F,P}/I_{\rm F,A} \simeq \frac{l_{\rm P}}{l_{\rm A}} \frac{n_{0,\rm P}}{n_{0,\rm A}} \frac{n_{\rm f,P}}{n_{\rm f,A}} \frac{\langle\sigma v\rangle_{\rm P}}{\langle\sigma v\rangle_{\rm A}} \frac{f_{3\to2,\rm P}}{f_{3\to2,\rm A}}. \tag{4}$$

The path length with appreciable neutral density is longer across the beam footprint than across the plasma edge, so $l_{\rm P}/l_{\rm A} \sim 1/2$. Calculations by the UEDGE neutral transport code indicate that the neutral density a few centimeters outside of the last-closed flux surface (LCFS) is roughly 5×10^{10} cm^{-3} for a DIII-D condition [16]. This is about ten times larger than the typical injected neutral density (of the full, half and third-energy components) of 5×10^9 cm^{-3}, so $n_{0,\rm P}/n_{0,\rm A} \sim 10$. In the scrape-off region, the electron density is low so virtually all neutrals are in the ground state. Consequently, unlike in the beam, reactions with neutrals in excited donor states are negligible, so $\langle\sigma v\rangle_{\rm P}/\langle\sigma v\rangle_{\rm A} \sim 1/3$. On the other hand, in the beam, collisional deexcitation competes with radiative deexcitation but it is negligible at the plasma edge, so $f_{3\to2,\rm P}/f_{3\to2,\rm A} \sim 1.5$. Combining these factors, the ratio of passive FIDA light to active FIDA light is roughly three times the ratio of edge-to-core fast-ion density, $I_{\rm F,P}/I_{\rm F,A} \sim 3(n_{\rm f,P}/n_{\rm f,A})$.

Under ordinary circumstances, the edge fast-ion density is much smaller than the core fast-ion density. Both Coulomb collisions and charge-exchange losses suppress the edge fast-ion density. For example, for the NSTX condition discussed in the next section, the $1/e$ energy loss time due to Coulomb scattering is 36 ms in the core but ~2 ms near the edge. Also, for orbits that traverse the scrape-off region, charge-exchange losses further deplete the density, with a typical decay time of ~1 ms. Consequently, $n_{\mathrm{f,A}}/n_{\mathrm{f,P}}$ is usually large, which implies that the active FIDA light is much brighter than the passive FIDA light. On the other hand, when instabilities transport fast ions to the edge, the edge fast-ion density can transiently equal the core fast-ion density. During these events, the passive FIDA light can exceed the active FIDA emission.

Similar calculations for the ratio of passive FIDA light to beam emission yield

$$I_{\mathrm{F,P}}/I_{\mathrm{B}} \simeq \frac{l_{\mathrm{P}}}{l_{\mathrm{A}}}\frac{n_{0,\mathrm{P}}}{n_{0,\mathrm{A}}}\frac{n_{\mathrm{f,P}}\sigma_{1\to 3}v}{(n_3/n_1)}\frac{1}{A_{32}+A_{31}}. \tag{5}$$

Ordinarily, the edge fast-ion density is small and this ratio is of $O(10^{-3})$ but, when the edge fast-ion density is large, the passive FIDA intensity is comparable to the intensity of beam emission (section 5).

4. Passive FIDA light of classical origin

During neutral-beam injection, some particles ionize at locations that result in orbits that strike the wall on their first full orbit. At DIII-D, these 'prompt losses' are detected by the BILD diagnostic [11]. The clearest indication of these losses occurs during modulation of the neutral-beam sources. For particular values of plasma current and toroidal field, the loss orbit 'connects' the location of neutral-beam deposition to the location of the BILD detector. Conceptually, the collisionless orbit links the small phase-space volume associated with the neutral-beam footprint and injection velocity to the small phase-space volume associated with the detector location and collimating apertures. Prompt losses from a particular source are observed when a classical orbit establishes a connection. In practice, the BILD detector has observed modulated prompt losses from every DIII-D neutral-beam source although, for some of the sources, losses are only rarely observed.

A special type of discharge was developed to observe this phenomenon [11]. In these discharges, the plasma current I_{p} slowly ramps up and down in a triangular waveform to alter the loss orbits. Meanwhile, each of the 8 neutral-beam sources injects a short 10 ms beam blip into the plasma once every 160 ms. Figure 2 shows an example of a discharge from the 2010 campaign that was used to calibrate a new scintillator-based fast-ion loss detector (FILD) [17]. Every time one of the 150-degree beams inject, the BES signal jumps up due to beam emission from the beam (figure 2(*c*)). In contrast, the BILD signal only measures large jumps in signal when the tangentially oriented beam at 210° (called '210RT') injects into a plasma with $I_{\mathrm{p}} \simeq 1.2$ MA (figure 2(*d*)).

Figures 3(*a*) and (*b*) show why signals appear on the BILD detector when the 210RT beam injects into a 1.2 MA plasma. The 210RT beam injects in the counter-current direction. Full-energy neutrals that ionize in the outer part of the plasma are born on trapped orbits. During the initial part of the orbit the particle travels clockwise in the counter-current direction but, after it reaches its turning point, it reverses direction and travels in the co-current direction. The particle strikes the BILD detector while traveling in the co-current direction on the outer leg of its banana orbit. At this point, the ion has precessed toroidally the ~150° between the deposition position and the BILD detector. In equilibria with lower values of I_{p}, the orbit does not advance as far toroidally by the time it reaches the wall, so the BILD diagnostic only detects prompt losses from the 210RT beam for $I_{\mathrm{p}} \simeq 1.2$ MA.

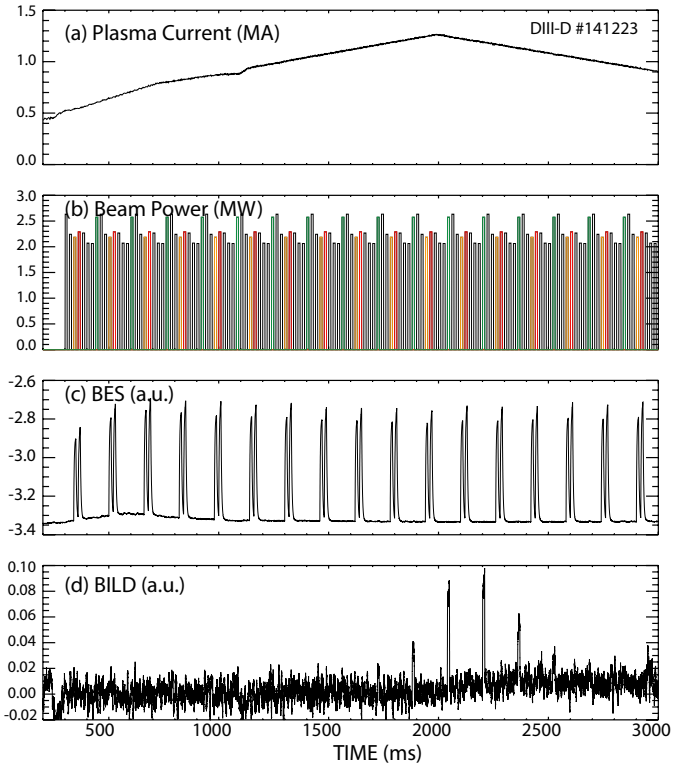

Figure 2. Time evolution of (*a*) plasma current I_p, (*b*) beam power from the 8 modulated sources, (*c*) 'slow' data from BES channel #42 and (*d*) the co-current BILD foil in a DIII-D discharge. Each pair of BES spikes occur when the two 150° beams are pulsed on; the BILD spikes occur when the 210RT beam is pulsed. Toroidal field $B_T = 2.0$ T; electron density $\bar{n}_e = 2 \times 10^{13}$ cm^{-3}.

The same phenomenon is observed by the BES diagnostic. Figure 4 shows an expanded version of BES data in the same discharge. At particular values of I_p, clear signals are observed when a particular beam injects; in this case, the 210RT beam. (The rounded waveform is an artifact associated with the low-pass filter employed with the 'slow' BES channels. Presumably, the true BES waveform is a square pulse like the beam pulse.) Note that this signal occurs when the 150° beams in the BES sightlines are off, so the signal cannot arise from beam emission. (In principle, light from beam emission could be reflected into the BES sightline—this effect was observed by an imaging diagnostic [18]—but, in this case, reflection of blue-shifted beam-emission light is disallowed by the viewing geometry.) When one BES channel observes a beam blip, all the other channels do too. Blips from the 210RT beam are observed for several values of plasma current. Blips from the 30° and 330° beams are most evident at low values of plasma current ($I_p \simeq 0.6$ MA).

Figures 3(*c*) and (*d*) show why signals appear on the BES channels when the 210RT beam injects into a 1.0 MA plasma. For this value of I_p, trapped orbits created by 210RT cross the plasma edge on their co-current leg near the toroidal location of the BES lens. Loss ions that charge exchange in the edge plasma produce the correct (blue-shifted) Doppler shift for detection. The diagnostic is observing passive FIDA light from loss orbits. In general, the BES prompt loss signals are observed for a wider range of I_p values than the BILD signals because the effective sensitivity of the BES diagnostic is wider in fast-ion phase space than the sensitivity of the small, collimated BILD foil.

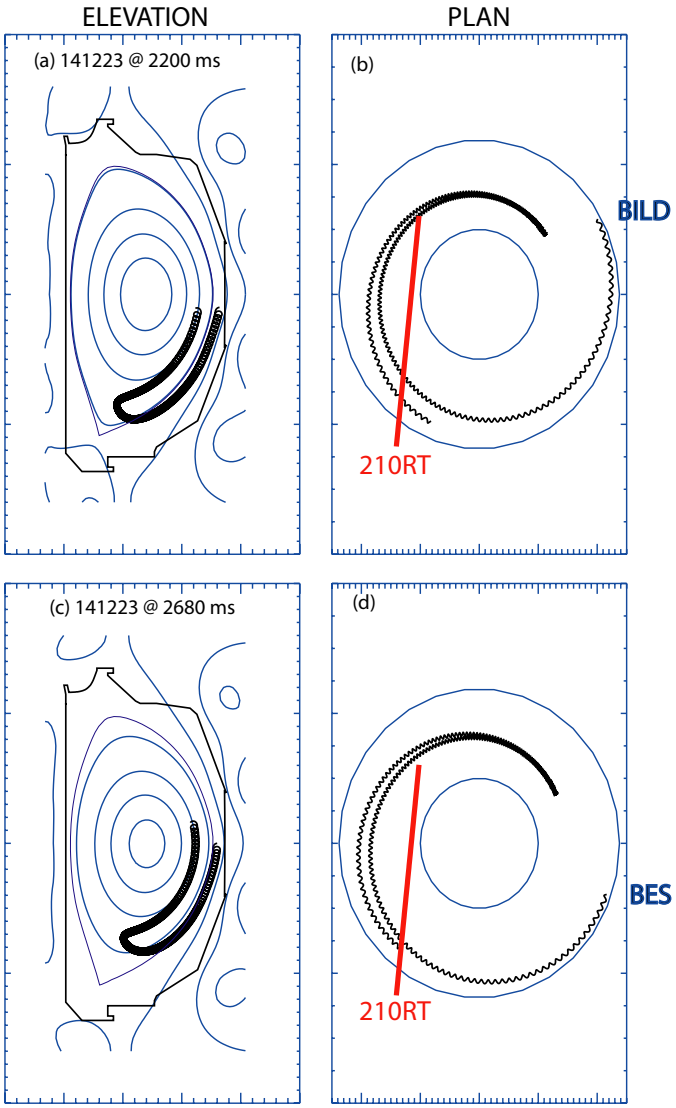

Figure 3. Projections of calculated orbits in the equilibrium fields at two different times for the discharge shown in figure 2. At 2200 ms (*a*), (*b*), a neutral that ionizes in the 210RT neutral-beam footprint with the velocity of the injected 80 keV neutrals executes a trapped orbit that strikes the BILD foil. At 2680 ms (*c*) and (*d*), neutrals that ionize in the 210RT footprint execute a trapped orbit that ends at the near edge of the BES sightlines.

The amplitude of the prompt-loss signals are $\sim 1/100$ of the beam-emission signals from the 150° beams. This is about ten times larger than the expected order of magnitude of passive FIDA light relative to beam emission for these conditions. The beam emission is given by equation (2). For the passive FIDA light, assume that the density of fast ions traversing the edge region is comparable to the injected neutral density. (Only a fraction of injected neutrals ionize onto loss orbits, which makes the density smaller, but, once ionized, they travel on a tortuous path rather than a straight line, which makes the density higher.) From equation (5),

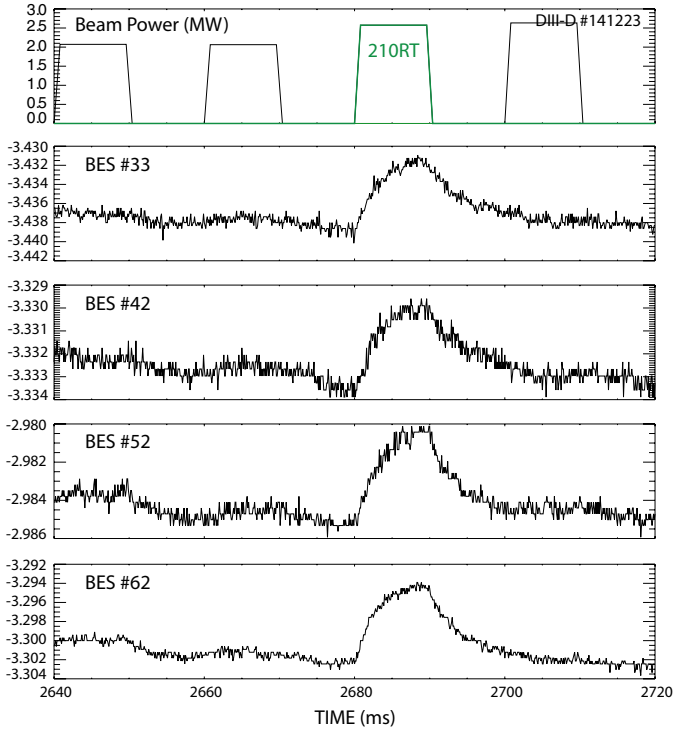

Figure 4. Details of the time evolution of neutral-beam power and signals from four BES 'slow' channels in the discharge shown in figure 2.

the expected ratio is roughly

$$I_{\mathrm{F,P}}/I_{\mathrm{B}} \simeq \frac{l_{\mathrm{P}}}{l_{\mathrm{A}}}\frac{n_{0,\mathrm{P}}}{n_{0,\mathrm{A}}}\frac{n_{\mathrm{f,P}}\sigma_{1\to3}v}{(n_3/n_1)}\frac{1}{A_{32}+A_{31}}.$$
$$\sim \frac{n_{0,\mathrm{P}}\sigma_{1\to3}v}{(n_3/n_1)(A_{32}+A_{31})}$$
$$\sim \frac{(5\times10^{10})(10^{-17})(3\times10^{8})}{(10^{-3})(10^{8})}$$
$$\sim 10^{-3},$$

or about an order of magnitude smaller than the observed ratio.

Fast-ion orbits in the equilibrium fields also produce passive FIDA light in NSTX. Figure 5 compares BES and SSNPA signals in an NSTX discharge with beam modulation. For these data, the signals are dc-coupled with no filtering so, if the signals came entirely from active sources, the waveforms would jump abruptly when the beams switch on or off. Core BES signals (figure 5(*c*)) show the expected abrupt jumps. Abrupt jumps are also observed on the SSNPA (figure 5(*a*)) and edge BES (figure 5(*b*)) signals (for example, when the beams turn off at 0.22 s) but the signals do not drop to the baseline level. Rather, after the abrupt drop, the signals decay on a few millisecond timescale; similarly, the risetime when a beam turns on is also a few milliseconds. The similarity between the SSNPA signal (figure 5(*a*)) and the edge BES signal (figure 5(*b*)) is striking. Both signals appear to contain both active and passive components. The passive FIDA feature is most evident on the BES channel that barely

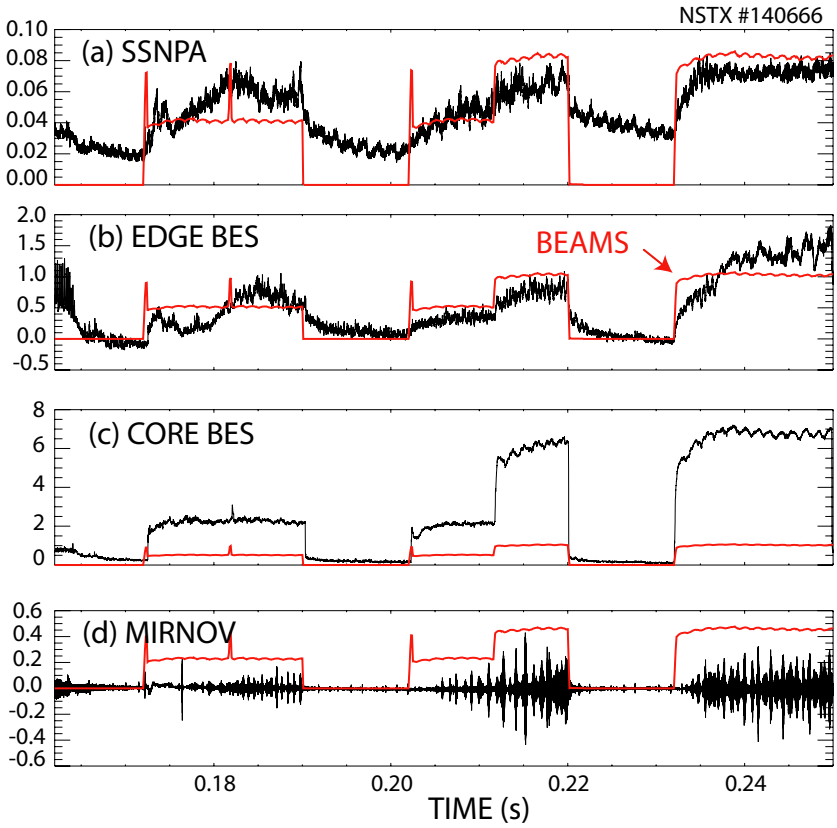

Figure 5. Time evolution of signals in volts from (*a*) an SSNPA channel, (*b*) a BES channel that intersects the beam near the plasma edge ($R = 142$ cm), (*c*) a BES channel that intersects the beam in the core ($R = 130$ cm) and (*d*) a Mirnov coil in an NSTX discharge with $I_p = 0.7$ MA, $B_T = 0.37$ T and $\bar{n}_e = 2.5 \times 10^{13}$ cm^{-3}. The density at $R = 130$ cm is 1.7×10^{13} cm^{-3}, while the sightline at $R = 142$ cm intersects the steep gradient region near the LCFS. Timing waveforms for injection by neutral-beam sources B and C at 90 keV are overlaid on the data; the spikes in the beam waveforms are artifacts.

penetrates the plasma (figure 5(*b*)) because the beam emission is small in the low density region at the plasma edge. In contrast, for a core channel that intersects the beam where the density is appreciable (figure 5(*c*)), the beam emission is an order of magnitude larger than the passive FIDA contribution.

NSTX is a spherical tokamak with a low toroidal field (3.7 kG in this case). Consequently, the gyroradius of the fast ions exceeds 10 cm. Many ions that are born on confined drift orbits traverse the edge region on the outer half of a gyro-orbit. During these excursions, the ions pass through a high neutral-density region where the probability of a charge-exchange reaction is high. These ions produce passive contributions to the SSNPA signal and passive FIDA light that is detected by the BES diagnostic. When a beam turns off, the population that produces these signals decays away with a characteristic charge-exchange loss time of $1/(n_0\sigma_{1\rightarrow 1}v) \simeq 1$ ms. When a beam turns on, the population of these edge-traversing fast ions approaches a steady state on a similar timescale. From equation (5), if one assumes an edge neutral density of 5×10^{10} cm^{-3} and that the density of edge-traversing fast ions is 10% of the central fast-ion density computed by TRANSP, the expected ratio of passive FIDA light to BES light for this

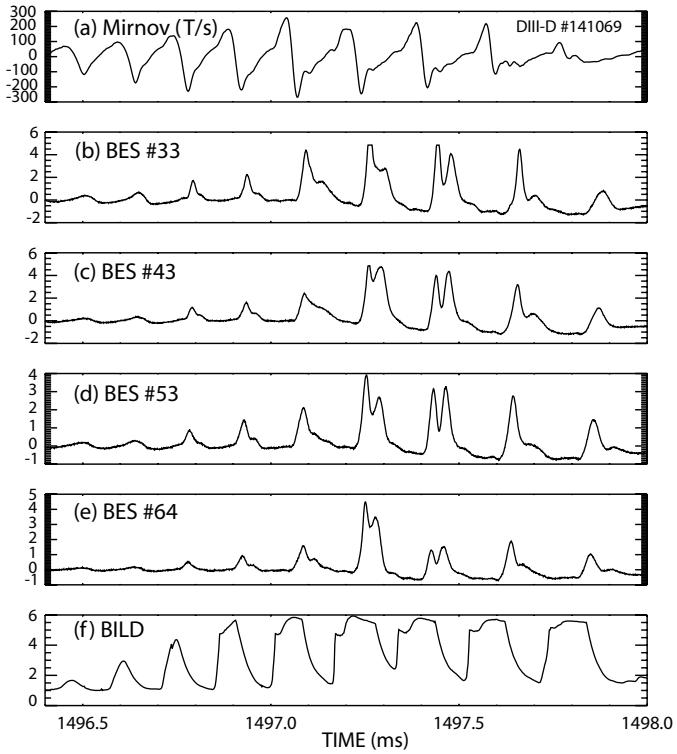

Figure 6. Time evolutions of (*a*) a Mirnov coil signal, (*b*)–(*e*) 'fast' data from four BES channels, and (*f*) the co-current BILD foil during an off-axis fishbone burst on DIII-D. $I_p = 1.0$ MA; $B_T = 1.7$ T; $\bar{n}_e = 3.7 \times 10^{13}$ cm^{-3}.

condition is a few percent. Experimentally, the ratio of the putative FIDA signal to the core beam-emission signal is $\sim 0.3/6 = 5\%$, in good agreement with the theoretical estimate.

5. Passive FIDA light during instabilities

Figure 6 shows an example from DIII-D of BES signals during an instability that expels fast ions from the plasma. In this discharge, both 150° beams were off, so there is no contribution of beam emission to the signal. Nevertheless, the peak signals are large (as large, in fact, as the beam emission measured between fishbone bursts in subsequent discharges). The instability is an $n = 1$ off-axis fishbone similar to the one observed in JT-60U [19] (n is the toroidal mode number). A detailed discussion of fast-ion transport by these modes is reported elsewhere [20], so only a brief summary is given here. Five different edge fast-ion diagnostics observe the losses. Losses occur in a burst once per wave period and have a particular phase relative to the mode, like the 'beacon' of losses observed during fishbones on the poloidal divertor experiment (PDX) [21, 22]. This beacon has an $n = 1$ structure and propagates in the co-current (counter-clockwise) direction. Figure 6(*f*) shows the periodic bursts measured by the BILD diagnostic. Unfortunately, for this fishbone burst, the BILD signal often saturates but data from weaker bursts show that the losses retain the same phase relationship with respect to the mode on every wave cycle. Both data from the FILD scintillator and theoretical considerations indicate that the lost particles are primarily trapped particles on the co-going leg of their orbit.

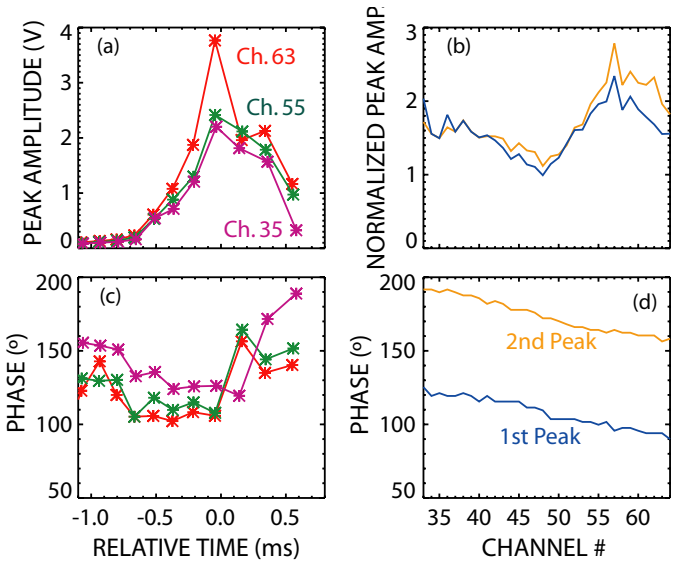

Figure 7. Reduced data for the off-axis fishbone burst shown in figure 6. Time evolution of the (*a*) amplitude and (*c*) phase of the largest spike during each fishbone period for three BES channels. (The phase is measured relative to the Mirnov coil signal.) Peak (*b*) amplitudes and (*d*) phases for the entire linear array for the pair of bursts observed from 1497.4–1497.5 ms. The measured voltage is divided by a correction for the differing sensitivities of the channels and by the calculated length of the line-of-sight through the edge region.

Four representative signals from the 32-channel linear BES array are shown in figure 6. Above a small threshold, all channels observe spikes at every wave cycle. This particular burst has a relatively small amplitude; on larger-amplitude bursts, most of the BES channels saturate. On many cycles, a pair of peaks that are separated by $\sim 50^\circ$ appears. This feature does not occur on the other loss diagnostics.

The hypothesis that these bursts are caused by passive FIDA light when the beacon of fast ions passes through the BES sightlines explains the data. The BES diagnostic is acting as an edge loss detector. Two peaks occur per cycle because the sightline crosses the edge at two locations. Figure 7 shows detailed analysis of the data from the 32-channel array in this burst. The amplitude of the bursts grows rapidly as the mode amplitude grows (figure 7(*a*)), just as it does on the other loss diagnostics. Figure 7(*c*) shows the phase of the largest burst in a cycle for three channels. When the largest signal originates from the same edge, the phase is nearly constant, as it is for the other loss diagnostics. When the largest signal originates from the other edge, the phase jumps $\sim 50^\circ$, which is the approximate toroidal separation of the two edges. As expected, the bursts are observed on all channels (figure 7(*b*)). The principal variation in signal amplitude is associated with variations in the length of the line-of-sight through the edge region; the data in figure 7(*b*) are divided by the relative length of the line-of-sight. (The data in figure 7(*b*) are also corrected for variations in light collection efficiency and detector gain.) The normalized signals tend to be slightly higher for more vertical views. Calculations indicate that the more vertical views are more sensitive to escaping trapped particles than the more tangential views (figure 8(*a*)), so the modest increase in signal for more perpendicular views is expected. All channels observe a phase difference of 50°–60° between the two bursts (figure 7(*d*)), consistent with the nominal toroidal separation of the two edges. An interesting feature of the data is the large variations in the relative amplitude of the two peaks (figure 6).

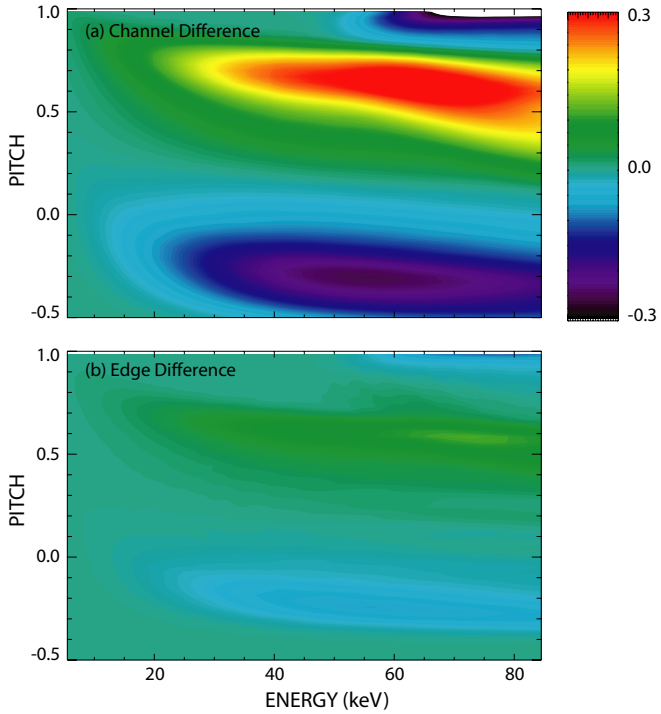

Figure 8. Difference in sensitivity to different parts of fast-ion velocity space for (*a*) different chords in the array at the near edge and (*b*) the same chord in the array at the near and far edges. The differences are normalized to the maximum sensitivity of BES channel #33 at the near edge. (The weight function for this case is shown in figure 1(*e*).) In (*a*), the difference ($\#33_{\mathrm{near}}$–$\#64_{\mathrm{near}}$)/max($\#33_{near}$) is shown; in (*b*), the difference ($\#33_{\mathrm{near}}$–$\#33_{\mathrm{far}}$)/max($\#33_{\mathrm{near}}$) is shown. The figures show that there is a modest difference in velocity-space sensitivity across the BES linear array, with the more perpendicular chords being more sensitive to perpendicular velocity, while there is very little difference in velocity-space sensitivity between the two edge regions.

Calculations show that the two edges are sensitive to similar parts of velocity space (figure 8(*b*)) but the edges are at different heights. Presumably, these variations indicate that the escaping ions have slightly different heights and velocities on successive cycles.

For these off-axis fishbones, the passive FIDA signals are the same order of magnitude as the beam emission. From the measured drop in the neutron rate at this burst, ∼10% of the fast ions are lost. If we assume that, in the beacon, the fast-ion density approaches the core fast-ion density, then equation (5) predicts comparable passive FIDA and beam-emission intensities.

Similar bursts occur when a 150° beam is on (figure 9). If one mistakenly interprets the bursts as a local density fluctuation, the BES signals imply core density fluctuations $\delta n_{\mathrm{e}}/n_{\mathrm{e}} \gtrsim 60\%$, which is clearly unphysical and inconsistent with, for example, the ∼2% fluctuation in the density interferometer signals.

Spectral measurements are not available for the BES viewing geometry but a vertically viewing spectrometer measures a passive FIDA feature within the spectral region accepted by the BES bandpass filter. (Note that, since the viewing geometry is different, the loss orbits and Doppler shifts measured by the spectrometer are not identical to those seen by the BES channels.) Figure 10 compares active FIDA spectra in the absence of fishbone bursts with

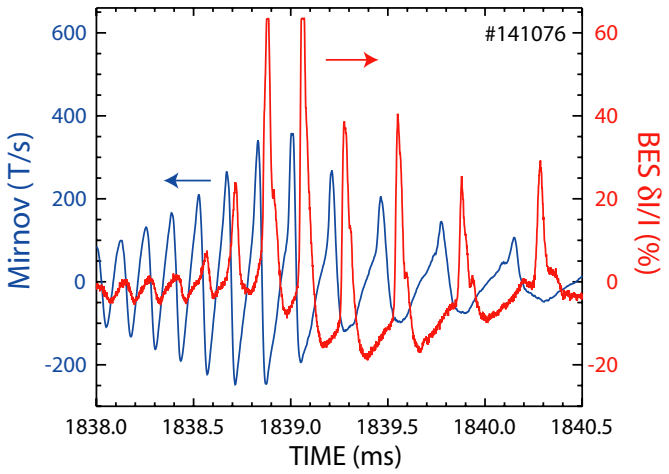

Figure 9. Time evolution of a Mirnov coil signal and 'fast' BES channel #53 during an off-axis fishbone burst that occurs while one of the BES active beams is injecting. The fast BES signal δI is normalized by the dc beam emission I.

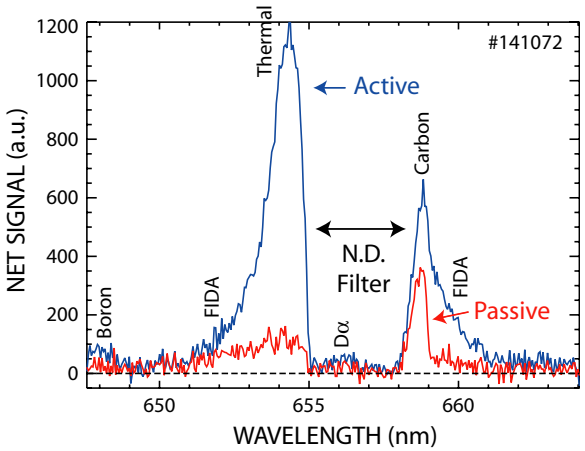

Figure 10. Spectra obtained by a vertically viewing FIDA spectrometer in a discharge with off-axis fishbone activity. The spectrum labeled 'active' is the difference between the signal when the active beam is on and when it is off (in the absence of fishbone activity). The spectrum labeled 'passive' is the difference between the signal at the time of fishbone activity and the signal just before the fishbone burst (with the active beam off throughout). This spectrometer has a narrow optical density neutral-density filter that attenuates the cold D_α line at 656.1 nm. Features in the spectrum are identified by vertical labels. The data are the average of six 1 ms time bins acquired near the time of three similar fishbone bursts. The BES bandpass filter measures blue-shifted light on the left side of the spectrum.

passive FIDA spectra acquired during fishbone bursts. This spectrometer [12] has relatively poor spectral resolution (∼0.5 nm) and employs a neutral-density filter that attenuates the cold D_α line at 656.1 nm to avoid detector saturation. The active spectrum has several features. The bump near 648 nm is a boron active charge-exchange line. The FIDA contribution to the spectrum is a broad feature that extends from 650 to 662 nm. At smaller Doppler shifts, thermal deuterium emission dominates. A carbon line appears at 658.3 nm. As expected, the

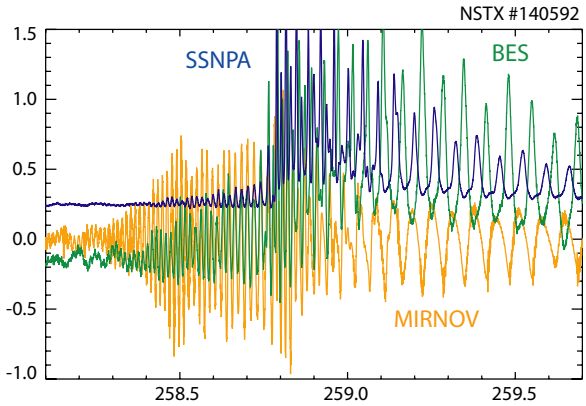

Figure 11. Time evolution of a Mirnov, SSNPA, and BES signal at a TAE burst that triggered a low-frequency fishbone in NSTX. $I_p = 0.76$ MA; $B_T = 0.50$ T; $\bar{n}_e = 2.7 \times 10^{13}$ cm^{-3}; sources A and B at 90 keV.

boron line and the thermal features are absent from the passive spectrum but the FIDA feature is still present, as is the carbon line. The passive blue-shifted spectrum is dominated by FIDA emission, confirming our interpretation of the bandpass-filtered BES signals.

The oscillations during off-axis fishbones are unusually large. More commonly, the passive FIDA signal at a burst is comparable to the fluctuations in the beam emission. Figure 11 shows an example from NSTX. In this case, the initial instability is a frequency-chirping toroidicity-induced Alfvén eigenmode (TAE) that triggers a lower-frequency, frequency-chirping, fishbone-like mode [23]. (In figure 11, the rapid early oscillations in the Mirnov signal are the TAE, while the longer-period oscillations after 259 ms are the fishbone.) These modes cause bursts in the SSNPA signal. As is usual for a fishbone, the SSNPA bursts occur once per cycle with a definite phase relative to the wave. The BES signal appears to be a superposition of oscillations at the wave frequency and positive bursts that have a definite phase relative to the wave. During the TAE phase, the signal is probably dominated by local fluctuations in the beam emission. In the fishbone phase, the passive FIDA bursts appear dominant but beam-emission fluctuations seem evident too. The neutron rate drops 19% at this event.

In addition to coherent fluctuations at the wave frequency, instabilities can modulate the passive FIDA light incoherently. Figure 12 shows signals during an NSTX TAE 'avalanche' [24] that caused an 18% drop in neutron emission. A reference f-FIDA signal that does not view a heating beam has spikes at each TAE avalanche, suggesting a contribution from passive FIDA light. The BES signals also have spikes at each burst. Detailed examination of one of these bursts shows that, as in the previous example, the BES signal seems to be the superposition of two contributions. One part consists of bipolar oscillations that resemble the Mirnov signal. (The beating associated with multiple toroidal modes is evident in both signals.) These fluctuations presumably are caused by local density fluctuations. The bipolar oscillations 'ride' on top of the second contribution: an incoherent 'bump' in signal. The time evolution of the 'bump' is very similar to the incoherent bump on the f-FIDA diagnostic.

The likely explanation for this phenomenon is that the TAE avalanche transports fast ions toward the edge. There are probably direct losses at the event, including some coherent losses, but these do not occur in the portion of phase space detected by the BES diagnostic. Instead, after the avalanche transports ions near the edge, Coulomb collisions scatter fast ions into the

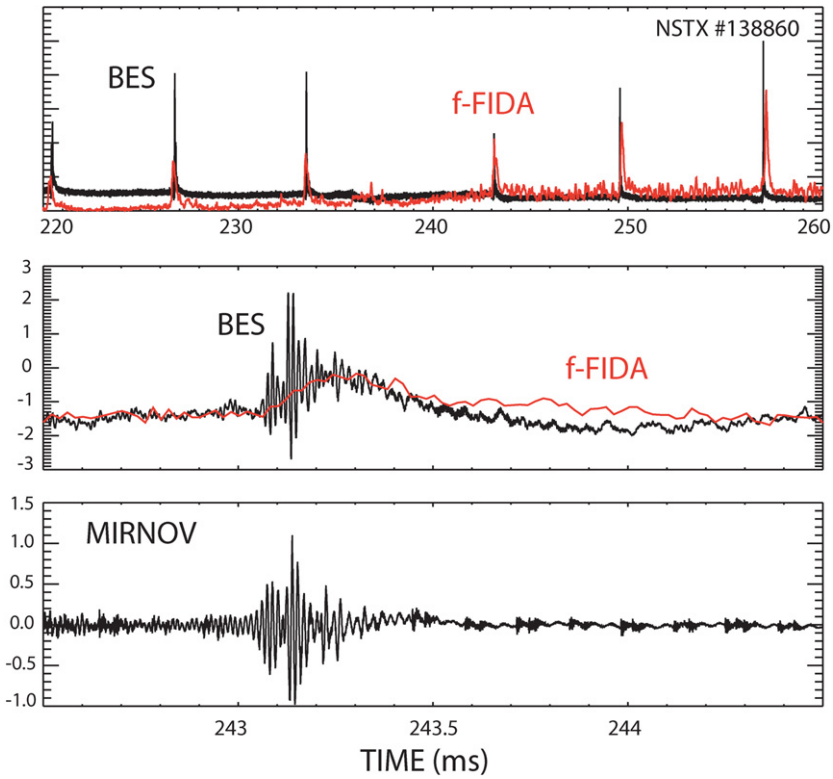

Figure 12. Time evolution of BES and reference f-FIDA signals in an NSTX discharge with TAE avalanches. $I_p = 0.73$ MA; $B_T = 0.40$ T; $\bar{n}_e = 2.4 \times 10^{13}$ cm^{-3}; sources A and B at 90 keV and source C at 70 keV.

BES sightline, causing a bump in signal that persists for a fraction of a millisecond. Incoherent bumps similar to these are often observed on edge fast-ion diagnostics. For example, for PDX fishbones, when an edge neutral-particle analyzer was tuned to measure high-energy ions in resonance with the mode, the signal consisted almost entirely of coherent oscillatons [21] but, at lower energies, the incoherent portion of the signal was largest [25], with a time evolution resembling the f-FIDA signal reported here. More recent examples of a mixture of coherent and incoherent losses are reported in [26, 27]. In the present case, the bump in signal is about 15% of the beam emission, consistent with a rough estimate based on equation (5).

6. Diagnostic implications

The previous sections present compelling evidence that BES signals can contain contributions from passive FIDA light. Even when the active beams are turned off, signals are detected from prompt losses (figure 4) and from confined orbits that traverse the scrape-off region (figure 5). When fast-ion driven instabilities expel fast ions, both coherent (figure 6) and incoherent (figure 12) bursts of signal are observed. Moreover, on theoretical grounds, passive FIDA signals are the correct order of magnitude to be detected (section 3).

The standard applications of BES diagnostics assume that local density fluctuations at the intersection of the sightline with the heating beam produce fluctuations in beam emission so, with corrections for atomic physics and volume-integration effects, the BES signal measures

low-k density fluctuations. Having established that passive FIDA signals are a potential contaminant to the normal signals, the question addressed here is: What effect does passive FIDA light have on the standard BES applications?

The primary application of BES diagnostics is the study of turbulent fluctuations. Low-k microinstabilities such as the ion-temperature gradient (ITG) instability produce a broad spectrum in the BES signals. It is very unlikely that passive FIDA light affects these measurements appreciably. The large orbits of fast ions make them less sensitive to turbulent electrostatic transport than thermal ions [28]. There is accumulating evidence that beam ions are transported by drift waves (especially in high temperature plasmas) [29, 30] but, even when the transport is measurable, it is at a much smaller level than for most fast-ion driven instabilities. Probably only a small fraction of ions are moved into the scrape-off region, so the expected ratio of passive FIDA to beam-emission light is tiny. Moreover, because of the non-resonant nature of the interaction, any fast-ion contribution is likely to be very low frequency, essentially dc. Consequently, measurements of turbulent fluctuations with BES are unaffected by passive FIDA contributions.

In contrast, determination of the mode structure of coherent fast-particle driven instabilities can be problematic during fast-ion expulsion. The data shown here demonstrate that the passive FIDA signal can be at least as large as the fluctuations in beam emission when large fast-ion losses occur. A reference view that misses the active beam can unambiguously distinguish beam-emission fluctuations from passive FIDA light. On DIII-D, because there are many heating beams, reference shots with the 150° beams turned off can check for passive FIDA light. Indeed, the reference discharge shown in figure 6 proves that the signals measured in other discharges are an admixture of passive FIDA and beam emission. For another instability, the energetic-particle geodesic acoustic mode (E-GAM) [31], a reference discharge without 150° beams shows that the passive FIDA contribution is negligible for this instability and the previously published [31] interpretation of the BES data is valid despite large fast-ion losses. In this case, the loss orbits are predominately large banana orbits that intersect the bottom of the machine before traversing BES sightlines.

NSTX currently has three neutral-beam sources, all of which are in the BES sightlines. It is not possible to turn off all of these sources without altering the instability under study, so additional techniques are needed to distinguish beam-emission fluctuations from passive FIDA light. One possibility is to install toroidally displaced, nominally identical, reference views, such as was done for the f-FIDA diagnostic. Comparison of the signals from the reference views with the active views would allow unambiguous determination of the passive FIDA contribution to the signals. Alternatively, since the passive FIDA contribution affects all channels similarly, analysis techniques that remove 'common-mode' contributions [3] could prove useful. In addition, time-scale separation techniques could distinguish fast bipolar instability fluctuations from the unipolar enhanced emission caused by slow fast-ion transport.

Finally, the observation of passive FIDA light provides new diagnostic opportunities. The techniques employed to study active FIDA light could be applied to diagnosis of the edge losses. Use of different bandpass filters could provide information on the energy of the losses. (Or, equivalently, adjustment of the angle of a single filter on repeat shots could scan the fast-ion energy [32].) Views from different angles could provide information on the pitch of the lost particles [33]. Vertical imaging [18] of the edge light could measure the poloidal distribution of the losses. In all of these applications it will be important to select spectral bands that are free of impurity lines.

With a quantitative understanding of the signals, one can envision using passive FIDA light as an edge neutral-density diagnostic. For example, to ensure that the flux of escaping fast ions is known accurately, the viewing geometry could be selected to detect prompt losses

deposited by a heating beam. The radial profile of edge FIDA light could then be used to infer the radial profile of the edge neutral density.

Another potential application is to use edge helium light to infer alpha-particle losses in ITER. In both JET [34] and TFTR [35], active charge-exchange recombination spectroscopy diagnosed confined high-energy alpha particles. If alpha particles escape from the core to the edge in ITER, a burst of passive helium light will occur. Equation (1) provides an estimate of the intensity of the signal. Assume the following:

- a tangential view through the edge with $\Delta l \simeq 2.5\,\mathrm{m}$,
- the edge neutral density is similar to DIII-D ($n_0 \simeq 5 \times 10^{10}\,\mathrm{cm}^{-3}$),
- a virulent burst, so that the edge fast-ion density transiently equals the core alpha density ($n_\mathrm{f} \simeq 3 \times 10^{11}\,\mathrm{cm}^{-3}$),
- detection of the $n = 4 \rightarrow 3$ transition of singly ionized helium at 468 nm, with 1/2 of the light at usable wavelengths ($\langle \sigma v \rangle \simeq 2 \times 10^{-10}\,\mathrm{cm}^3\,\mathrm{s}^{-1}$).

Then the predicted radiance is $\sim 10^{15}$ photons $\mathrm{cm}^{-2}\,\mathrm{s}^{-1}$, which is comparable to the radiance of beam emission in DIII-D. If challenges associated with backgrounds and reflected light can be overcome, light from edge alphas can be detected in ITER.

In summary, data from both DIII-D and NSTX show that passive FIDA light is detected by BES diagnostics. This light can complicate BES measurement of the eigenfunction of fast-ion driven instabilities, although additional measurements and new analysis techniques may resolve any ambiguities. The existence of bright passive FIDA light affords new opportunities for the diagnosis of fast-ion losses.

Appendix. Calculation of the passive FIDA weight function

Because of the low electron density, nearly all edge neutrals are in the ground state. Consequently, in contrast to the active FIDA signal, where donors in excited states contribute appreciably to the number of atoms left in the $n = 3$ state, only reactions with ground-state donors are important. The edge neutrals are sufficiently cold that the relative velocity is approximately the fast-ion velocity. Thus, the reaction rate is proportional to $\sigma_{1\rightarrow 3} v$ and this quantity depends only on the fast-ion energy, independent of pitch.

The sightline geometry determines the direction of emitted photons $\hat{p}$. The Doppler shift depends on the angle between $\hat{p}$ and the fast-ion velocity $\vec{v}$. The fast-ion distribution function is given in terms of energy E and pitch $v_\parallel / v$. The unit vector in the direction of the magnetic field $\hat{b}$ is found from the EFIT [36] reconstruction of the equilibrium magnetic field, evaluated at the intersection of the sightline with the edge. The parallel velocity component along $\hat{b}$ is determined by the energy and pitch. The remaining velocity components depend on the perpendicular velocity and the gyroangle. To compute the weight function for a particular value of E and $v_\parallel / v$, a set of uniformly spaced gyroangles are selected. For each gyroangle, $\vec{v}$ is computed, then the Doppler shift is determined from $\vec{v} \cdot \hat{p}$. Once the Doppler shift is known, the weight of this particle is proportional to the transmission of the bandpass filter at this particular wavelength. Stark splitting causes effective smearing over the filter transmission band. After summing the transmission over gyroangles, the weight at this value of energy and pitch is given by the transmission times the reaction rate $\sigma_{1\rightarrow 3} v$.

Acknowledgments

Eric Fredrickson and Michio Okabayashi alerted me (WWH) to the perplexing nature of the BES signals. Mike Van Zeeland first noted the diagnostic opportunities associated with passive

FIDA signals. Rejean Boivin suggested the potential ITER application and Dan Thomas gave helpful advice. Gary Porter and Mathias Groth provided the estimate of the edge neutral density. Ray Fonck and many others developed the NSTX BES diagnostic. None of the measurements would be possible without the dedicated support of the DIII-D and NSTX teams. This work was funded by the US Department of Energy under SC-G903402 and DE-FC02-04ER54698 and by DE-FG03-02ER54681 and DE-FG02-06ER54867.

References

[1] Fonck R J, Duperrex P A and Paul S F 1990 *Rev. Sci. Instrum.* **61** 3487
[2] Gianakon T A, Fonck R J, Callen J D, Durst R D and Kim J S 1992 *Rev. Sci. Instrum.* **63** 4931
[3] Durst R D *et al* 1992 *Rev. Sci. Instrum.* **63** 4907
[4] Durst R D *et al* 1992 *Phys. Fluids* B **4** 3707
[5] Gupta D K, Fonck R J, Mckee G R, Schlossberg D J and Shafer M W 2004 *Rev. Sci. Instrum.* **75** 3493
[6] Smith D R *et al* 2010 *Rev. Sci. Instrum.* **81** 10D717
[7] Heidbrink W W, Burrell K H, Luo Y, Pablant N A and Ruskov E 2004 *Plasma Phys. Control. Fusion* **46** 1855
[8] Heidbrink W W 2010 *Rev. Sci. Instrum.* **81** 10D727
[9] Ogawa K *et al* 2008 *Plasma Fusion Research* (rapid communications) **3** 30
[10] Heidbrink W W *et al* 2007 *Plasma Phys. Control. Fusion* **49** 1457
[11] Zhu Y B, Heidbrink W W and Pickering L D 2010 *Nucl. Fusion* **50** 084024
[12] Luo Y, Heidbrink W W, Burrell K H, Gohil P and Kaplan D 2007 *Rev. Sci. Instrum.* **78** 033505
[13] Liu D *et al* 2006 *Rev. Sci. Instrum.* **77** 10F113
[14] Podesta M, Heidbrink W W, Bell R E and Feder R 2008 *Rev. Sci. Instrum.* **79** 10E521
[15] Heidbrink W W, Liu D, Luo Y, Ruskov E and Geiger B 2011 *Commun. Comput. Phys.* at press
[16] Groth M *et al* 2005 *J. Nucl. Mater* **337** 425
[17] Pace D C *et al* 2010 *Rev. Sci. Instrum.* **81** 10D305
[18] Van Zeeland M A, Heidbrink W W and Yu J 2009 *Plasma Phys. Control. Fusion* **51** 055001
[19] Matsunaga G *et al* 2009 *Phys. Rev. Lett.* **103** 045001
[20] Heidbrink W W, Austin M E, Fisher R K, Matsunaga G, McKee G R *et al* 2011 Characteristics of off-axis fishbones *Plasma Phys. Control. Fusion* submitted
[21] Beiersdorfer P, Kaita R and Goldston R J 1984 *Nucl. Fusion* **24** 487
[22] White R B *et al* 1983 *Phys. Fluids* **26** 2958
[23] Fredrickson E D *et al* 2006 *Phys. Plasma* **13** 056109
[24] Fredrickson E D *et al* 2009 *Phys. Plasma* **16** 122505
[25] Heidbrink W W and Sadler G J 1994 *Nucl. Fusion* **34** 535
[26] Nagaoka K *et al* 2008 *Phys. Rev. Lett.* **100** 065005
[27] García-Muñoz M *et al* 2010 *Phys. Rev. Lett.* **104** 185002
[28] Naitou H, Kamimura T and Dawson J M 1979 *J. Phys. Soc. Japan* **46** 258
[29] Heidbrink W W, Murakami M, Park J M, Petty C C and Van Zeeland M A 2009 *Phys. Rev. Lett.* **103** 175001
[30] Günter S *et al* 2007 *Nucl. Fusion* **47** 920
[31] Nazikian R *et al* 2008 *Phys. Rev. Lett.* **101** 185001
[32] Van Zeeland M A *et al* 2010 *Nucl. Fusion* **50** 084002
[33] Muscatello C M, Heidbrink W W, Taussig D and Burrell K H 2010 *Rev. Sci. Instrum.* **81** 10D316
[34] von Hellermann M G *et al* 1993 *Plasma Phys. Control. Fusion* **35** 799
[35] McKee G *et al* 1995 *Phys. Rev. Lett.* **75** 649
[36] Lao L L, St John H, Stambaugh R D, Kellman A G and Pfeiffer W 1985 *Nucl. Fusion* **25** 1611